Article:
West, Ryan John Hatcher, Briggs, Laura, Fjeldstad, Maria Perona et al. (2 more authors) (2018) Sphingolipids Regulate Neuromuscular Synapse Structure and function in Drosophila. Journal of comparative neurology. ISSN 0021-9967

https://doi.org/10.1002/cne.24466

Sphingolipids Regulate Neuromuscular Synapse Structure and function in Drosophila

Journal:	*Journal of Comparative Neurology*
Manuscript ID	JCN-17-0268.R2
Wiley - Manuscript type:	Research Article
Keywords:	Drosophila, neuromuscular junction, sphingolipids, Basigin, synapse

Sphingolipids Regulate Neuromuscular Synapse Structure and function in *Drosophila*

Running Title: sphingolipid, synapse structure and function

Ryan J. H. West[1]*, Laura Briggs[1]* Maria Perona Fjeldstad[2], Richard R. Ribchester[2] and Sean T. Sweeney[1]

1. Department of Biology and Hull York Medical School, University of York, Wentworth Way, Heslington, York, YO10 5DD UK

2. Euan MacDonald Centre for Motor Neurone Disease Research and Centre for Discovery Brain Sciences, University of Edinburgh, 1 George Square, Edinburgh EH8 9JZ, UK.

Correspondence: Sean T. Sweeney, Department of Biology, University of York, Wentworth Way, Heslington, York, UK YO10 5DD

Email sean.sweeney@york.ac.uk Tel: 01904 328537

Abbreviated Title (58 characters) Sphingolipids regulate *Drosophila* synapse structure and function

*These authors contributed equally

Acknowledgement for support: This work was supported by the award of MRC grants G0400580 and MR/M013596/1to STS.

Associate Editor: Ian Meinertzhagen

Figures: 7

Keywords: neuromuscular junction, lipid rafts, synaptic bouton, synaptic adhesion

Abbreviations:

NMJ	Neuromuscular Junction
HRP	Horse Radish Peroxidase
TEM	Transmission Electron Microscopy
SPT1	Serine Palmitoyl Transferase
SPTLC1/2	Serine Palmitoyl Transferase Light Chain 1/2
EMS	ethyl methyl sulphonate
HSAN1	Hereditary Sensory and Autonomic Neuropathy Type 1
LSD	Lysosomal Storage Disease
TOF	Train of Five

Abstract (222 words)

Sphingolipids are found in abundance at synapses and have been implicated in regulation of synapse structure, function and degeneration. Their precise role in these processes, however, remains obscure. Serine Palmitoyl-transferase (SPT) is the first enzymatic step for synthesis of sphingolipids. Analysis of the *Drosophila* larval neuromuscular junction revealed mutations in the SPT enzyme subunit, *lace/SPTLC2* resulted in deficits in synaptic structure and function. Although neuromuscular junction (NMJ) length is normal in *lace* mutants, the number of boutons per NMJ is reduced to ~50% of the wild type number. Synaptic boutons in *lace* mutants are much larger but show little perturbation to the general ultrastructure. Electrophysiological analysis of *lace* mutant synapses revealed strong synaptic transmission coupled with predominance of depression over facilitation. The structural and functional phenotypes of *lace* mirrored aspects of *Basigin* (*Bsg*), a small Ig-domain adhesion molecule also known to regulate synaptic structure and function. Mutant combinations of *lace* and *Bsg* generated large synaptic boutons, while *lace* mutants showed abnormal accumulation of Bsg at synapses, suggesting that Bsg requires sphingolipid to regulate structure of the synapse. In support of this, we found Bsg to be enriched in lipid rafts. Our data points to a role for sphingolipids in the regulation and fine-tuning of synaptic structure and function while sphingolipid regulation of synaptic structure may be mediated via the activity of Bsg.

Introduction

In 1967, Derry and Wolfe (Derry and Wolfe, 1967) identified a prominent enrichment of glycosphingolipids within synaptic structures in the mammalian brain. To date our understanding of the role of these enigmatic lipids in synapse structure and function has yet to be fully elucidated. Sphingolipids are major lipid components of the plasma and endomembrane system and have been implicated in many forms of neuropathy and neurodegeneration (for review see (Sabourdy et al., 2015)). Sphingolipids are proposed to generate structure in membranes due to their rigidity and association with cholesterol (see (Munro, 2003)). They are also known to be potent signalling molecules regulating processes such as apoptosis, proliferation, migration and responses to oxidative stress (reviewed in (Lahiri and Futerman, 2007)).

Numerous neurological and neurodegenerative conditions are directly attributable to the inability to synthesise or catabolise sphingolipids. The failure to synthesise all or particular sphingolipids gives rise to a number of neurological conditions such as infant-onset symptomatic epilepsy (loss of GM3 ganglioside synthesis (Simpson et al., 2004), bovine spinal muscular atrophy (loss of 3-ketohydrosphingosine reductase (Krebs et al., 2007) and hereditary sensory and autonomic neuropathy type 1 (HSAN1; recessive and dominant mutations in serine palmitoyl transferase subunit 1 (*SPTLC1* (Bejaoui et al., 2001; Dawkins et

al., 2001)). Conversely failure to catabolise sphingolipids in the lysosome generates a subset of lysosomal storage diseases/disorders (LSD's) known as sphingolipidoses, of which there are approximately 14 identified separate genetic conditions (reviewed in (Kacher and Futerman, 2006)). Sphingolipids are now suggested to have a prominent role in the onset and progression of Alzheimer's disease (Grimm et al., 2005) while the production after bacterial infection of autoimmune antibodies to gangliosides present at the neuromuscular synapse is likely to cause the dramatic and often lethal paralysis seen in Guillain-Barré and Miller-Fisher syndromes (Roberts et al., 1994; Willison et al., 1997). The presence of sphingolipids at the synapse is further attested by the ability of tetanus and botulinal toxins to effect their entry to synapses via co-attachment to synaptic glycosphingolipids (Nishiki et al., 1996; Deinhardt et al., 2006).

While the presence of sphingolipids (in particular, glycosphingolipids) at the synapse is well established, little is known about their functional or structural role in the operational life of the synapse. Some in vitro studies have addressed the role of sphingolipids at synapses in the context of sphingolipid/cholesterol microdomains and indicate roles in the function and localisation of neurotransmitter receptors, (Brusés et al., 2001; Hering et al., 2003) and synaptic exocytosis (Salaün et al., 2005; Darios et al., 2009; Chan and Sieburth, 2012; Chan et al., 2012). The prominence of sphingolipids in neurological disease suggests that absence or accumulation of sphingolipids can exert an influence in synaptic function and indicates an inappropriately large gap in our knowledge

regarding the actions of these lipids at the synapse. In the above outlined context, roles for sphingolipids in synapse structure and function remain to be determined. To this end, we have undertaken an analysis of sphingolipid function at a model synapse, the third instar neuromuscular junction of *Drosophila*. We have examined mutations in *SPT2*/*SPTLC2* (Serine Palmitoyltransferase, Long Chain Base Subunit 2), which encodes an essential subunit of the Serine Palmitoyltransferase (SPT) heterodimer necessary for the initial step in sphingolipid synthesis, for defects in neuromuscular synapse structure. We present evidence to suggest that sphingolipids are essential for synaptic structure and function, and structural regulation may be mediated partially through function of the Ig domain adhesion protein Basigin/CD147 (Bsg).

Materials and Methods

Fly stocks and Maintenance

Drosophila stocks were raised on standard yeast, sugar and agar medium at 25°C (4% yeast, 8% sucrose, 1.2% agar, 3.6 mM calcium chloride, 0.65g/l ferrous sulphate, 6.5 g/l potassium sodium tartrate, 0.4 g/l sodium chloride and 0.4 g/l manganese chloride, 0.065% Nipagin, 0.0005% Bavistin). *Spt2/lace* alleles were a kind gift from John Roote (The University of Cambridge, UK), *hiw* stocks were gifted by Aaron DiAntonio (Washington University, USA) and *UAS-lace-HA*, $lace^{k05305}$ and $lace^{2}$ were a gift from Takashi Adachi-Yamada (Gakushuin University, Japan), *Bsg* mutants and rescue transgenes were a gift

from Anne Ephrussi (EMBL, Heidelberg). All other stocks were obtained from the Bloomington *Drosophila* Stock Center.

Immunohistochemistry

Third instar wandering larvae were dissected in PBS and fixed in 3.7% formaldehyde/PBS for 7 min. Following washes larvae were stained using the appropriate antibody in 0.1% PBT. Primary antibodies were used at the following concentrations Cy3 conjugated α-HRP (1:200, goat, Jackson ImmunoResearch, Stratech Scientific), α-syt (1:2000, rabbit, (West et al., 2015)), α-nc82 (1:50, mouse, DSHB), α-dlg (1:50, mouse, DSHB), α-GluRIIb (1:2500, rabbit, a kind gift from Aaron DiAntonio, Washington University, St Louis Missouri, (Marrus et al., 2004) DiAntonio et al, 1999), α-Bsg (1:200, Rat, a kind gift from Anne Ephrussi, EMBL, Heidelberg (Besse et al., 2007)). Cy3, Cy5 and FITC conjugated secondary antibodies were used at 1:200 (goat, Jackson ImmunoResearch, Stratech Scientific). A comprehensive list of antibodies can be found in supplementary table 1.

Electrophysiology

Intracellular microelectrode recordings were made from Muscles 6 and 7 in abdominal segments 3 and 4 of filleted third instar larval preparations bathed in HL3 saline, using standard techniques (Powers et al., 2016). The concentrations of Ca^{2+} and Mg^{2+} in the saline were reduced (to 0.4 mM and 10 mM respectively) in order to depress mean quantal content of EJPs (Excitatory junction potential

(evoked transmitter release)), thereby increasing sensitivity to differences in synaptic strength between the *Drosophila* lines we tested (Dodge and Rahamimoff, 1967)(Guan et al., 2017). The reduced EJP amplitude under these conditions also obviated correction of EJP amplitudes for non-linear summation (McLachlan and Martin, 1981). Preparations were mounted in a recording chamber (bath volume approximately 1 ml) on the stage of an Olympus BX50WI upright, fixed stage microscope and visualised using 10x or 20x water-dipping objectives. Glass capillary microelectrodes with resistances 15-40 MΩ were pulled using a Brown-Flaming P87 puller (Sutter Instruments, Novato, USA), filled with 3M KCl and mounted on an MP-85 Huxley-type micromanipulator (Sutter Instruments). The reference electrode was an Ag/AgCl pellet connected to the system ground. Membrane potentials were recorded using pClamp 10 (Clampex) software via an HS2A headstage (0.1x gain) connected to a Geneclamp 500 amplifier and Digidata 1550B interface (all Molecular Devices, Sunnyvale, USA). Segmental nerves were aspirated into a micropipette with a heat-polished tip, aperture 10-15 µm, and stimulated with trains of four or five (TOF) supramaximal pulses (nominally 10V, 0.1-0.2 ms duration; interval 50 ms, ie 20Hz; programmed in Clampex) triggering a DS2 stimulator (Digitimer, Welywn Garden City, UK). Three pulse trains were delivered at 5 s intervals and each train was preceded by either a positive or negative rectangular 100 ms, 1 nA current pulse delivered through the recording microelectrode. The voltage deflection (after subtraction of electrode resistance) was used to calculate input resistance and qualitatively check membrane time constant as indicators of

membrane integrity. Recordings from muscles with input resistances less than 1.5 MΩ or time constant less than 5 ms were rejected (Powers et al., 2016). Spontaneous EJPs (miniEJPs) were recorded in the absence of nerve stimulation over a period of up to 60s. EJP recordings were analysed using pClamp 10.6 and miniEJPs were measured using Minianalysis (Synaptosoft, Atlanta, USA). Mean frequency of miniEJPs was estimated from the inverse of their mean intervals. EJP and miniEJP amplitudes were corrected to an arbitrary standard membrane potential of -65 mV before calculating quantal content by the direct method (Ribchester, 2011). An index of synaptic facilitation (*f*: positive values indicating facilitation, negative values indicating depression) was calculated from the change in quantal content of the first (m_1) and either the fifth (m_5) or occasionally the fourth EJP, according to the formula $f=m_5/m_1-1$.

Imaging and Quantification

Imaging and quantification of synaptic structure was performed as described in (West et al., 2015). Briefly, synaptic bouton numbers at muscles 6/7 hemisegment A3, were determined by counting each distinct, spherical, anti-synaptotagmin–positive varicosity contacting the muscle. As synaptic bouton number has been shown to increase proportionally with muscle surface area synaptic bouton numbers were normalized against muscle surface area by dividing the bouton number by the muscle surface area and multiplying by mean wild-type muscle surface area as described by (Milton et al., 2011). Muscles and synapses were imaged at room temperature using a camera (AxioCam HRC) on

an inverted fluorescence microscope (Axiovert 200; Carl Zeiss) using Plan Neofluar 10×/0.3 NA and 40×/0.75 NA lenses, with Axio- Vision Rel. 4.8 software (Carl Zeiss). Measurements were made from images using ImageJ (National Institutes of Health). Confocal images were obtained using a confocal microscope (LSM 710 Axio Observer Z1; Carl Zeiss). Z-stacked images of single NMJ's were obtained using a Plan Apochromat 63×/1.4 NA oil objective. Z-stack projections of muscle 4 NMJ's were analyzed using ImageJ to quantify bouton diameter, NMJ length, and satellite bouton number. Bouton diam- eter was measured as the width across a bouton at the widest point (Milton et al., 2011). NMJ length was measured using the NeuronJ ImageJ plugin.

Transmission electron microscopy was performed as described previously in (West et al., 2015). Third instar wandering larvae were dissected and fixed in 0.1 M $NaPO_4$, pH 7.4, 1% glutaraldehyde, and 4% formaldehyde, pH 7.3, overnight. Fixed larval preparations were washed 3× in 0.1 M $NaPO_4$ before incubation in OsO_4 (1% in 0.1 M $NaPO_4$; 2 h). Preparations were washed 3× in distilled water before incubation in 1% uranyl acetate. Preparations were washed (3× distilled water) and dehydrated through a graded ethanol series; 20% increments starting at 30% followed by two 100% changes and then 2× 100% propylene oxide. Preparations were incubated in a graded series of epon araldite resin (in propylene oxide); 25% increments culminating in 3× 100% changes. Individual muscles were then dissected out. These were then transferred into embedding molds, and the resin was polymerized at 60°C for 48 h. Resin mounted preparations were sectioned (60–70 nm) using glass knives upon a microtome

(Ultracut UCT; Leica) and placed onto grids. Preparations were subsequently incubated in uranyl acetate (50% in ethanol), washed in distilled water, and incubated in lead citrate. Sections were imaged using a transmission electron microscope (TECNAI 12 G^2; FEI) with a camera (Soft Imaging Solutions MegaView; Olympus) and Tecnai user interface v2.1.8 and analySIS v3.2 (Soft Imaging Systems). Quantification of active zone length, number of synaptic vesicles localized within 250 nm of the T-bar active zone, synaptic vesicle diameter and mitochondrial size was performed using ImageJ. Representative images were taken from at least 3 animals per genotype.

Lipid Raft Extraction and Western Blotting

Methodology for purification of lipid rafts was adapted from (Fernandez-Funez et al., 2009) and (Zhai et al., 2004). Briefly 50 third instar larvae of (w^{1118}) were sonicated in 250 μl cold TNET buffer (100 mM Tris, 0.2 mM EGTA, 150 mM NaCl, 0.3 M Sucrose, pH 7.5, 1% Triton-X, 1x protease inhibitor) and incubated on ice for 30 min.. Debris was removed by centrifugation at 3000g for 10 min. and 200 μl of crude supernatant extract mixed with 400 μl of 60% Optiprep™ in 5 ml. 5% Optiprep™ was underlaid with 1.8 ml 30% Optiprep™ which was underlaid by the Optiprep™ and extract mixture in 5.1 ml ultracentrifuge tubes. Gradients were spun at 43,865 RPM for 1 hour at 4°C in a Beckman Coulter Optima™ L-100 XP Ultracentrifuge using a VTi90 Rotor. Following centrifugation 10 500 μl fractions were collected from the bottom and analysed via western

blotting. Antibodies against the α Subunit of the Na^+/K^+ ATPase (1:100,000, mouse, DSHB) and Syntaxin (1:50, mouse, DSHB) were used as negative and positive controls for lipid rafts, respectively. Anti-Bsg (1:1500, rat) was a kind gift from Dr. Anne Ephrussi (EMBL Heidelberg, Germany). HRP-conjugated secondary antibodies were from Cell signaling technology. A comprehensive list of antibodies can be found in supplementary table 1.

Results

SPTLC2/*lace* function is Essential in *Drosophila*

SPT acts in the first enzymatic step in the de novo synthesis of sphingolipids, catalysing the condensation of L-serine with palmitoyl-coA to generate 3-ketosphinganine and further subsequent sphingolipid derivatives. SPT is composed of two subunits, SPTLC1 and SPTLC2. Previously we have demonstrated that expression of *Drosophila* SPTLC1 (dSPT1) bearing a neomorphic mutation associated with HSAN1, and aberrant sphingolipid production, induced morphological aberrations in synapse growth at the *Drosophila* third instar larval Neuromuscular Junction (NMJ) (Oswald et al., 2015). In order to determine the role of sphingolipids in the regulation of synaptic morphology we looked to characterise further the role of *SPTLC2* in regulating the structure and growth of the *Drosophila* larval neuromuscular synapse. Lethal and hypomorphic mutations in the *Drosophila SPTLC2* gene*, lace,* have

previously been identified (Ashburner, 1982; Adachi-Yamada et al., 1999). Here, using iPCR, we mapped the insertion sites of the two *P*-element insertions within the *lace* locus (Figure 1). *l(2)lac*^{k05305} was mapped to 97 nucleotides upstream of the start ATG codon while *l(2)lacW*^{K00706} mapped 52 nucleotides downstream of the first exon (Figure 1b). The *lace*^{2} allele has previously been identified as an EMS induced point mutation leading to the amino acid change S429N (Sasamura et al., 2013). The *lace*^{8} allele is an additional EMS induced mutation while *lace*^{1} is a spontaneous mutation (Ashburner, 1982). Using this series of mutants, we screened for allelic combinations that generated an early/late pupal lethality (Figure 1a), giving an optimal penetration of the phenotype and a reduction in sphingolipid content for an analysis of the 3rd instar NMJ. *Lace*^{k05305}*/lace*^{2} transheterozygotes and *lace*^{k05305} homozygotes were identified as giving an optimal lethal phase for studying synaptic growth and structure. In addition it has previously been demonstrated that l*ace*^{k05305}*/lace*^{2} transheterozygotes and *lace* ^{k05305} homozygotes present with just 5.5% and 2.5% sphingolipid content (Herr et al., 2003), respectively, compared to wildtype. A schematic of the *lace* alleles utilised in this study is given in Figure 1b. All mutant combinations were found to be lethal.

lace Mutants Display Aberrant NMJ Structure

Using the *Drosophila* third instar larval NMJ as a model synapse we identified both transheterozygous and homozygous *lace* mutants displaying significant

perturbations to gross morphological NMJ structure. This was characterised by a significant decrease in synaptic bouton number coupled with an increase in bouton size (Figure 2a-e). It was also observed that mutants showed the presence of spur-like structures emanating from terminal boutons (Figures 2d), suggesting either partially formed synaptic extensions, or collapse of a bouton. *Lace* mutants showed no significant variance in the length of the NMJ arbour or muscle surface area when compared to wildtype (Figure 3a-b).

Despite significant perturbations at the gross morphological level, at a sub-cellular level pre- and post- synaptic structures appear unperturbed, with no observable alteration to either the pre-synaptic active zone marker nc82/bruchpilot or post-synaptic markers GluRIIA and Discs-large (DLG) (Figure 3c-e). There was also no difference in Futsch or FasII (Supplementary Fig. 1). Mutants did, however, show an apparent disruption to plasma membrane antigens recognised by the anti-horse radish peroxidase (HRP) antibody, leading to an uneven distribution of HRP labelling (Figure 2d, 3c-e, and supplementary Fig. 2a). Perturbed HRP staining was not observed in wildtype animals.

At an ultrastructural level individual synaptic components also appear normal (Figure 3f-j), showing no significant aberration to active zone size, synaptic vesicle number or synaptic vesicle size (Figure 3h-j). One notable observation, however, is the number of enlarged mitochondria observed throughout the nervous system of *lace* mutants (Fig. 3g, Supplementary Fig. 2.). No significant difference in the total number of mitochondria was observed between genotypes

(data not shown). Taken together these initial findings suggest that sphingolipid is essential for maintaining synapse structure at a gross morphological level.

NMJ Length is Maintained With Fewer Boutons in the Absence of Sphingolipids

Boutons are added to the neuromuscular junction during progression through the larval instars (Zito et al., 1999). The counting of boutons commonly stands proxy for NMJ size in many studies of the larval neuromuscular junction (Schuster et al., 1996). On initial observation, the *lace* mutant NMJ appeared to be of normal length despite having a reduced bouton count. Having identified a defect in bouton structure, we then examined NMJ length in relation to bouton structure. By counting boutons per NMJ arbour while simultaneously measuring the length of the NMJ we found that in sphingolipid depleted NMJ's the overall length of the NMJ was indistinguishable from wildtype while boutons per NMJ was found to be significantly reduced by ~50%, compared to wild-type (Figures 2 and 4a-c). *lace* mutants showed no reduction in muscle surface area (Figure 3h), indicating that reduced bouton number was not as a result of reduced muscle size. Branching patterns of NMJ's were also indistinguishable between sphingolipid depleted NMJ's and wild-type (Figure 4d).

To ascertain whether sphingolipid deficient *lace* mutant NMJ's were capable of further synaptic growth, we combined the $lace^{k05305}/lace^{k05305}$ mutant with the

synaptic overgrowth mutant *highwire* (*hiw*) (Wan et al., 2000; Collins et al., 2006). NMJ's in the hiw^{ND9};$lace^{k05305}$/$lace^{k05305}$ mutant combination were found to be capable of growth well above wildtype length (Fig 5). In the *hiw/lace* mutant combination, boutons per unit-length were generated at around 50% of the *hiw* figure alone. This is similar to the comparison between wild-type and *lace* where *lace* produces ~50% less boutons per unit length compared to wild-type. Collectively this data indicates a defect in NMJ synaptic structure, but not overall NMJ length regulation, in the absence of sufficient sphingolipid.

Expression of lace Rescues Synaptic Structure

Having ascertained that sphingolipid is essential to the generation or maintenance of mature synaptic structure, we examined the relative sphingolipid contribution of the pre- and post-synaptic compartments. To facilitate this, we employed the $lace^{k05305}$/$lace^{k05305}$ mutant and rescued lace function in either the pre-synaptic compartment alone, using the pan-neuronal *elav*-GAL4 driver, or the post-synaptic compartment alone, using the muscle expressing *MHC*-GAL4 driver. We also performed a global rescue using *Tubulin*-GAL4 driven expression of UAS-*lace*. Here we found that presynaptic expression of lace (*elav*-GAL4) failed to recover bouton structure or number in the $lace^{k05305}$/$lace^{k05305}$ background (Figure 5). In contrast rescue of lace function in the post-synaptic muscle compartment induced a nearly complete rescue of both reduced synaptic bouton number and bouton enlargement (Figure 5). Global expression of UAS-

lace was sufficient to completely rescue all aspects of NMJ perturbation in *lace* mutants (Figure 5). We also examined a role for glia in the sphingolipid regulation of NMJ structure. Glial expression of lace, using the *repo*-gal4 driver, was sufficient to rescue both reduced synaptic bouton number and enlarged bouton size in $lace^{k05305}/lace^{k05305}$ mutants (supplementary figure 3). Interestingly the post-synaptic rescue of lace function induced the formation of excessive 'satellite' boutons (Figure 5d). Satellite boutons are small boutons sprouting from the main synaptic arbour (Beumer et al., 1999; Koh et al., 2004; Marie et al., 2004). These data suggest a partial non-cell-autonomous role for sphingolipids in the regulation of synaptic growth and structure. Feeding *Drosophila* larvae sphingosine, the product of serine palmitoyl transferase activity can rescue some phenotypes caused by loss of SPT (Adachi-Yamada et al., 1999). Our data points to an ability to rescue the sphingolipid deficiency NMJ phenotype with global, muscular or glial expression, but not neuronal expression.

lace mutants show increased synaptic strength

Sphingolipids have previously been implicated in the synaptic vesicle cycle (Salaün et al., 2005; Darios et al., 2009; Chan and Sieburth, 2012; Chan et al., 2012) and in the localisation and function of neurotransmitter receptors (Brusés et al., 2001; Hering et al., 2003). Having observed significant perturbations to NMJ morphology, but not ultrastructure, we carried out an electrophysiological analysis in *lace* mutants to determine the role that sphingolipids might play in the regulation of synaptic activity.

Mutant *lace* larvae showed a significant increase (~50%) in both evoked EJP amplitude (Figure 6a-b, Supplementary Tables 2&3) and quantal content (Figure 6c) at both muscles 6 and 7, compared to wild-type controls. No significant difference in input resistance or resting membrane potential was observed between genotypes (Figure 6d-e). Expression of lace under the control of the global driver *tubulin*-Gal4 was sufficient to alleviate both elevated evoked EJP amplitude and quantal content in *lace* mutant larvae (Figure 6b-c). At the Ca^{2+}/Mg^{2+} concentrations used in the present experiments, consistent synaptic facilitation during Train-of-Five (TOF) stimulation was observed in wildtype larvae but not in *lace* mutants (Figure 6f). Specifically, *lace* mutant larvae show a consistent and constant EJP size during the TOF stimulus at NMJs in both muscles 6 and 7, compared to wild-type larvae (Figure 6f). This difference in EJP consistency during the TOF stimulus was partially rescued by global (*tubulin*-Gal4) expression of lace in the *lace* mutant background (Figure 6f). Mutant *lace* synapses also showed a significant increase in mini frequency (Muscle 7, Figure 6g) and Quantal size (Muscle 6, Figure 6h), compared to wildtype. These phenotypes, however, were not rescued by expression of wildtype lace (*tubulin*-Gal4, Figure 6g-h).

lace Mutants Reveal a Relationship Between lace and Basigin in the regulation of synapse structure.

Previous studies have identified that the Ig family protein Basigin/CD147 (Bsg) is required pre- and post-synaptically to restrict synaptic bouton size and regulate

bouton number. *Bsg* mutants were shown to display significantly enlarged boutons and a reduction in synaptic bouton number, while the overall NMJ size remained close to wild-type (Besse et al., 2007), a phenotype similar to *lace*. *Bsg* mutants also show an elevated evoked EJP amplitude, mini amplitude and mini frequency similar to *lace* mutants (Besse et al., 2007) with an additional release asynchrony. As with sphingolipids, *Bsg* has also been implicated in the regulation of actin cytoskeleton dynamics, with mutants showing accumulation of mitochondria (Curtin et al., 2005), perturbed synaptic structure and an early lethal phase (Besse et al., 2007). As such we asked whether a functional interaction existed between *Bsg* and the loss of sphingolipid function generated in *lace* mutants and whether Bsg localisation was also altered in *lace* mutants.

Here we show that heterozygous *lace*^{k05305}*/Bsg* mutant combinations phenocopy both *lace* and *Bsg* mutants, displaying an ~ 50% reduction in synaptic bouton number, coupled with significantly enlarged synaptic boutons (Figure 7 a-c). As has previously been shown (Besse et al., 2007) heterozygous mutations in either *Bsg* or *lace* alone show no variance from wildtype.

Having identified an apparent genetic relationship between *Bsg* and *lace* we next looked to determine the abundance and localisation of Bsg in *lace* mutants. Here we show that, as previously identified, Bsg is present at the NMJ. However we also demonstrate there to be a significant increase in the amount of Bsg accumulating at *lace* mutant NMJ's when compared to wildtype (Figure 7d-f). Relative HRP was also quantified as a control (Figure 7f) with no significant variance observed between *lace* mutants and wildtype.

Sphingolipids are major constituents of lipid rafts, specialised membrane microdomains that act to regulate membrane dynamics, endocytic process and cell signalling events, amongst other processes. Previous studies have implicated Bsg in the regulation of signalling complexes within lipid-raft like domains in cancer (Grass et al., 2013). We then proposed that the accumulation of Bsg observed at the NMJ of *lace* mutants may relate to its presence within lipid raft microdomains. To determine whether Bsg was present in microdomains in *Drosophila,* lipid rafts were isolated via optiprep gradient fractionation. The presence of Bsg within lipid raft fractions was confirmed by identification of its presence within floating fractions 9 and 10, which were also positive for the known lipid raft marker Syntaxin (Figure 7g) (Chamberlain et al., 2001; Lang et al., 2001). The transmembrane ion pump Na+/K+ ATPase, which is excluded from lipid rafts and enriched in non-lipid raft membranes (Fernandez-Funez et al., 2009), was not. Taken together these findings suggest that Bsg is localised within lipid raft micro-domains and that a functional interaction exists between sphingolipids and Bsg in the regulation of synaptic structure.

Discussion

The role of sphingolipids at synapses

The enrichment of sphingolipids at synapses has been long known (Derry and Wolfe, 1967). Assigning functions for these enigmatic lipids at the synapse has remained problematic. Ablation of gangliosides in mouse has identified subtle defects in neurotransmission (Zitman et al., 2008; 2010; 2011) while loss of G3-

ganglioside synthesis results in an infantile onset epilepsy (Simpson et al., 2004), the mechanism for which remains obscure. A specific role for sphingosine has been identified in promoting SNARE protein fusion and synaptic exocytosis (Darios et al., 2009).

Many sphingolipid species present in the outer leaflet of the plasma membrane are found in association with cholesterol as 'lipid rafts'. Neurons receive supplementary cholesterol from glia which is essential for supporting synapse maturation and additional synaptogenesis (Mauch et al., 2001) suggesting cholesterol, and potentially lipid rafts, are rate limiting for these processes. Depletion of both cholesterol and sphingolipids together has been shown to reduce and enlarge dendritic spines with eventual loss of synapses in hippocampal neurons in culture possibly due to reduced association with lipid rafts of synapse structure promoting proteins such as Post-Synaptic Density protein 95 (PSD95) (Hering et al., 2003). In this present study, we have reduced synthesis of sphingolipids with a mutation in *SPTLC2*, and examined the development of neuromuscular synapses in the *Drosophila* larval preparation. This approach has allowed us to study the genetic depletion of sphingolipids at an identified synapse *in vivo* and investigate a role for sphingolipids in the regulation of synaptic structure and activity. As part of this study, we have also identified a potential role for the Ig domain cell adhesion protein Bsg in sphingolipid dependent regulation of synaptic structure.

Sphingolipids are required for normal synapse structure

On examination of sphingolipid deficient synapses, we observed a disruption to the normal synaptic structure. We found that synaptic boutons were enlarged and the overall numbers of boutons reduced by ~50% while the length of the neuromuscular synapse remained indistinguishable from wildtype. This phenotype is highly reminiscent of the reduction of synapse number, but increase in synapse size observed in hippocampal neurons in culture depleted for lipid rafts (Hering et al., 2003). Nevertheless, we were surprised that beyond the structural deficit of the synapse, the ultrastructure of the synapse was remarkably intact, suggesting a role in fine-tuning of synaptic properties.

Synapses depleted for sphingolipids were capable of greater growth when combined with the synaptic overgrowth mutation *highwire* (*hiw*) (Wan et al., 2000). Our data suggests the mutations in *lace* and sphingolipid depletion decouples bouton structure from normal synaptic length. Large boutons are observed in mutants of *mothers against dpp (mad), thick veins (tkv), saxophone (sax) medea (med),* and *glass-bottom-boat (gbb)*, components of the TGF-ß pathway that is known to regulate synaptic growth (Aberle et al., 2002; Sweeney and Davis, 2002; Rawson et al., 2003; McCabe et al., 2004). However these mutations reduce synaptic length by ~50% and ultrastructural synaptic defects such as non-plasma membrane attached active zones (T-bars), large endosomal vesicles and ripples in pre-synaptic peri-active membranes are observed (McCabe et al., 2004). One obvious ultrastructural defect that is present in sphingolipid depleted synapses is enlarged mitochondria (Figure 3g,

supplementary figure 2). Enlarged mitochondria are observed in a number of sensory neuropathies (see (Vital and Vital, 2012) for review) and it is of interest that dominant mutations in *SPTLC1* (Bejaoui et al., 2001; Dawkins et al., 2001) and SPTLC2 (Penno et al., 2010; Oswald et al., 2015) that generate aberrant sphingolipids give rise to Hereditary and Sensory Neuropathy Type 1 (HSAN1) where enlarged mitochondria are often observed. This may be attributable to a recognised role for sphingolipids in mitochondrial fission (Ciarlo et al., 2010).

To dissect the spatial requirement for sphingolipid regulation of synapse structure we rescued the *lace* mutant with a rescue transgene, expressed globally, pre- or post-synaptically. We found that we could rescue synaptic bouton size and number with a global expression of the rescue transgene (Figure 5), but no aspects of the phenotype could be rescued with a pre-synaptic expression. Perturbed NMJ morphology could also be rescued by glial or post-synaptic expression of *lace*, however post-synaptic muscle expression generated a partial rescue, with an excess of 'satellite' boutons, a phenotype normally associated with integrin dysfunction (Beumer et al., 1999) or endocytic defects (Koh et al., 2004; Marie et al., 2004). Previous data feeding *lace* mutant larvae with sphingosine, the product of the SPT enzyme, partially rescued *lace* mutant associated phenotypes (Adachi-Yamada et al., 1999) Taken together with our analysis, there is a strong suggestion that sphingolipid precursors such as sphingosine may be able to act non-cell autonomously, and traffic between cells

to support synapse structure and function, but not when supplied from the nervous system.

Sphingolipids are required for regulation of synaptic output.

Analysis of EJP and miniEJP characteristics at the 3rd instar larval NMJ reveals mutations in *lace* produce, at the Ca^{2+}/Mg^{2+} concentrations we used, a small but significant increase in synaptic strength, accompanied by a change in short-term plasticity, with synaptic depression predominating over synaptic facilitation. NMJs with high-quantal content EJPs normally show synaptic depression during paired or short-train repetitive stimulation, while those with a low basal quantal content show synaptic facilitation (Lnenicka and Keshishian, 2000; Lnenicka et al., 2006). Further analysis is required, for instance using a range of Ca^{2+} concentrations, to establish whether this apparent change in synaptic plasticity is commensurate with a greater basal synaptic strength in the *lace* mutant larvae, or whether it represents a specific effect of the mutation, disrupting the normal link between mechanisms that couple basal quantal content to short-term synaptic plasticity.

In vitro and *in vivo* analysis has suggested a role for sphingolipids in synaptic vesicle endocytosis (Salaün et al., 2005; Shen et al., 2014) and exocytosis (Darios et al., 2009; Chan and Sieburth, 2012; Chan et al., 2012) in addition to a role in neurotransmitter distribution (Brusés et al., 2001; Hering et al., 2003). We observe no evident defects in neurotransmitter receptor distribution. Interestingly, ablation of major subsets of gangliosides and subsequent analysis of synaptic function at the NMJ in a mouse model reveals a more pronounced run-down of

neurotransmitter release upon sustained stimulation, consistent with the data we have presented here (Zitman et al., 2008; 2011). We cannot however, directly attribute the apparent deficit in synaptic facilitation we observed here in *lace* mutants to exo- or endocytosis, at this point.

Sphingolipids interact with Basigin to regulate synaptic structure at the synapse.

We noted a strong phenotypic similarity at the larval neuromuscular synapse between the *lace* mutants and mutations in the small Ig domain adhesion protein *Basigin/CD147* (Besse et al., 2007). Bsg is a glycoprotein localised in the plasma membrane that is known to genetically interact with integrins (Curtin et al., 2005) during development of the *Drosophila* eye. In *Bsg* mutants, synaptic boutons at the larval neuromuscular junction are enlarged in size and reduced in number with a modest reduction in synaptic span (Besse et al., 2007). Bsg has previously been localised to sphingolipid enriched lipid rafts in invading epithelial breast cells (Grass et al., 2013) and we observed that Bsg is abundant in the lipid raft associated membrane fraction, co-sedimenting with syntaxin, a known component of lipid rafts (Fernandez-Funez et al., 2009). We cannot say at this juncture if Bsg function is directly regulated by sphingolipids. Indeed, recruitment of Bsg to lipid rafts can be critical for the recruitment of other protein factors such as claudin-5 in retinal vascular epithelial cells (Arima et al., 2016). However, given the genetic interaction between *Bsg* and *lace*, with *bsg;lace* transheterozygous double mutants phenocopying both *lace* and *bsg* mutants, our

data suggests Bsg and sphingolipids genetically interact to regulate synaptic structure. We interpret this interaction as indirect; the loss of sphingolipid generated in the *lace* mutant affecting Bsg function to regulate synapse structure and function

Synaptic sphingolipids have previously been implicated in synaptic vesicle release (Darios et al., 2009; Chan and Sieburth, 2012; Chan et al., 2012), endocytosis (Salaün et al., 2005), neurotransmitter receptor localisation (Hering et al., 2003; Brusés et al., 2001) and maintenance of synaptic activity (Zitman et al., 2008; 2011). However other roles at the synapse for these enigmatic lipids remain elusive. Two potential functions for sphingolipid at the synapse are suggested by our study. Mitochondrial uptake of Ca^{2+} shapes Ca^{2+} dependent responses (Mammucari et al., 2018). The enlarged mitochondria we observe in *lace* mutants may impinge on Ca^{2+} uptake to affect synaptic facilitation. A further deficit in Ca^{2+} handling at the synapse is suggested by the recent finding that Bsg is an obligatory subunit of plasma membrane Ca^{2+}-ATPases (PMCAs). PMCAs extrude Ca^{2+} to the extracellular space, and knock-out of Bsg considerably affects Ca^{2+} handling by PMCAs (Schmidt et al., 2017). Sphingolipid deficient synapses in the *lace* mutant have deficits in Bsg function which may in turn have an effect on Ca^{2+} dynamics via PMCA function.

Ablation of sphingolipid synthesis at a *Drosophila* model synapse supports a role for sphingolipids in maintenance of synaptic activity and regulation of synaptic

structure. Our analysis also points to sphingolipid dependent regulation of synaptic structure via function of the small Ig-domain protein Bsg. The precise regulation of synapse structure and function is a potent mechanism underlying synaptic plasticity and we suggest that the presence of sphingolipids at synapse may partially reflect this function.

Acknowledgements: We thank the Bloomington *Drosophila* stock center, Developmental Studies Hybridoma Bank Iowa, the University of Cambridge, Department of Genetics Stock Centre, Thomas Hummel, Takashi Adachi-Yamada, John Roote, Aaron DiAntonio and Anne Ephrussi for antibodies and Drosophila stocks. Thanks also go to Meg Stark (Technology Facility, University of York, York, England, UK) for assistance with transmission EM and Dr Paul Pryor (University of York, UK) for his expertise and assistance with lipid raft isolation.

Conflict of Interest Statement

The authors declare no competing interests.

Author contributions

Data were collected by R.J.H.W., R.R.R., M.P.F, and L.B. All Authors contributed towards the design, implementation and analysis of the experiments. Statistical analysis and assembly of figures was performed by R.J.H.W and R.R.R. The manuscript was written by R.J.H.W., R.R.R and S.T.S.

References

Figure Legends

Figure 1. lace is Essential for Survival in *Drosophila*

a. Complementation analysis between *lace* mutants was used to identify allelic combinations that gave an optimal penetration, generating an early/late pupal lethality, for analysis of the 3rd instar neuromuscular junction. Percentages shown represent the number of unbalanced transheteroygous flies that eclosed for those crosses where transheterozygotes survived to adulthood, baseline = 50%.

b. Gene schematic showing the location of the two *P*-element insertions mapped to the lace locus in this study (*l(2)lacW*^{P05305} and *l(2)lacW*^{K00706}) as well as the previously mapped EMS induced *lace*^{2} mutation.

Figure 2. Loss of Sphingolipid Synthesis Leads to Enlarged Bouton Structure at the NMJ

a-b. *Drosophila* third instar larvae presenting with homozygous or transheterozgous mutations in *lace* display a significant reduction in synaptic bouton number (ANOVA $p < .001$, with post-hoc Dunnett's comparison to wildtype controls: *** $p < .001$). **c-e.** Reduced synaptic bouton number is coupled with a significant increase in mean synaptic bouton size, associated with an increased frequency of synaptic boutons displaying a surface area > 8 μm^2 in lace mutants. *lace* mutants also displayed spurr like protrusions from terminal boutons (arrow heads, a and d). Scale bars = 10 μm.

Figure 3. Synaptic Components Appear Unchanged in *lace* Mutants

a-b. *lace* mutants show no change in total NMJ length or muscle surface area. **a**; ANOVA; $p < .064$, **b;** ANOVA; $p < .616$.

c-e. Pre- (nc82) and post- (discs large and GluRII) synaptic markers appear unchanged at an immunohistochemical level in lace mutants. Scale bars = 5 μm.

f-j. Ultrastructural examination reveals no significant perturbation to active zone length (h), synaptic vesicle number (i) or synaptic vesicle diameter (j). Enlarged mitochondria (asterisk) are observed in lace mutants (g). Scale bars = 1 μm.

Figure 4. *lace* Mutants Are Capable of Further Synaptic Growth.

a-b. Combining *lace* mutants with the synaptic overgrowth mutant *highwire* revealed double mutants show a ~ 50% reduction in bouton number, compared to *Hiw* alone. This is comparable to the ~ 50% reduction observed in *lace* mutants, compared to wild type. *Hiw;lace* double mutants, however, remain capable of further synaptic growth showing a significant increase in synaptic length (**c**) and branching (**d**), comparable to that seen in *Hiw* single mutants. ANOVA $p < .001$, with post-hoc Dunnett's comparison to wildtype controls: *** $p < .001$ and Tukey between group's comparison: ### $p < .001$.

Figure 5. Aberrant Synaptic Architecture Can be partially Alleviated by Post- Expression of lace

a-c. Global (Tubulin-Gal4) expression of UAS-*lace* was sufficient to completely allieviate both the increase in synaptic bouton size (b) and reduction in synaptic bouton number (c) observed in lace mutants. Post-synaptic (*MHC*-Gal4) expression of UAS-*lace* elicits an almost complete rescue of both enlarged synaptic bouton size and reduced bouton number. Pre-synaptic (*Elav*-Gal4) expression of lace is insufficient to rescue aberrant synaptic architecture. **a.**

ANOVA; p < .001 with post hoc Dunnett's comparison to wildtype: *** p <.001, ** p < .01 and Tukey comparison within groups vs Gal4 control ### p <.001, ## p < .01 or vs lace mutant $$$ p <.001. **b.** ANOVA; p < .000 with post hoc Dunnett's comparison to wildtype: *** p <.001, and Tukey comparison within groups vs Gal4 control ### p <.001 or vs lace mutant $$$ p <.001.

Figure 6. *lace* mutants display increased synaptic strength

a. representative intracellular recording traces, showing evoked EJP responses to TOF stimulation and spontaneous (mini) EJPs.

b. *lace* mutant (*lace*^{k05305}/*lace*^{k05305}) larvae show significantly (ANOVA with post-hoc Tukey comparison between groups, ** p<.01) elevated evoked EJP amplitudes at muscles 6 and 7 compared to wildtype larvae and larvae expressing *lace* globally (tubulin-gal4) in a *lace* mutant background (rescues). Box and whisker plots demonstrate the median, interquartile range and the range of recorded values.

c. *lace* mutant (*lace*^{k05305}/*lace*^{k05305}) larvae show a significant increase (ANOVA with post-hoc Tukey comparison between groups, * p<.05, ** p<.01) in quantal content at muscles 6 and 7 compared to wildtype larvae and larvae expressing *lace* globally (tubulin-gal4) in a *lace* mutant background (rescues). Box and whisker plots demonstrate the median, interquartile range and the range of recorded values.

d-e. No significant variance in input resistance or resting membrane potential was observed between genotypes.

f. Synaptic facilitation index (*f*: positive values indicating facilitation, negative values indicating depression) calculated from the change in quantal content of the first (m_1) and either the fifth (m_5) or occasionally the fourth EJP, according to the formula $f=m_5/m_1-1$. Box and whisker plots demonstrate the median, interquartile range and the range of recorded values (ANOVA with post-hoc Tukey comparison between groups, * p<.05).

g. *lace* mutant ($lace^{k05305}/lace^{k05305}$) larvae show a significant (ANOVA with post-hoc Tukey comparison between groups, * p<.05) increase in spontaneous (mini) release frequency at muscle 7 compared to wildtype larvae. Box and whisker plots demonstrate the median, interquartile range and the range of recorded values.

h. *lace* mutant ($lace^{k05305}/lace^{k05305}$) larvae show a significant (ANOVA with post-hoc Tukey comparison between groups, * p<.05) increase in quantal size at muscle 6, compared to wildtype larvae. Box and whisker plots demonstrate the median, interquartile range and the range of recorded values.

Figure 7. *lace* Mutants Reveal a Functional Interaction Between Between lace and Basigin

a-c. Heterozygous *lace/Bsg* double mutants phenocopy both *lace* and *Bsg* transheterozygotes, displaying a significant reduction in synaptic bouton number

and enlargement of synaptic boutons**.** ANOVA; p < .001 with post hoc Dunnett'comparison to wildtype: *** p < .001, ** p < .01 and Tukey comparision within groups ### p< .001, # p < .05.

d-f. Bsg was shown to accumulate at NMJs in *lace* mutants, showing a significant increase in mean anti-Bsg fluorescence compared to wildtype. Mean relative HRP fluorescence was also quantified, as a control, and showed no variance from wildtype. Student's T-test; p < .000 (**d**) and p < .745 (**e**).

g. Gradient fractionation revealed to Bsg to be present within floating fractions 9 and 10, along with the lipid raft marker Syntaxin, demonstrating Bsg to be present in lipid raft microdomains in *Drosophila* larvae.

Supplementary Figure 1. Futsch and FasII are unperturbed in *lace* mutants

a-b. representative images showing no variance in the localisation of Futsch or FasII at the third instar NMJ between wildtype and lace mutant larvae. Scale bars; a = 2 μm, b = 10 μm.

Supplementary Figure 2. Enlarged Mitochondria in *lace* Mutants

a-b. Transmission electron micrographs showing enlarged mitochondria with axon bundles of lace mutant larvae. Scale bars, a = 2 μm, b = 500 nm.

c. Quanification of mitochondria size in wildtype and lace mutant larvae, wildtype; n = 15 axon bundles, N = 3 animals, lace; n = 18 axon bundles, N = 3 animals. Student t-test p < .01.

d. micrographs showing enlarged mitochondria (mito-GFP) within synaptic boutons of lace mutant larvae (arrow heads). Scale bar = 10 μm.

Supplementary Figure 3. Glial Expression of lace alleviates gross morphological NMJ defects in *lace* mutants, revealing a non-autonomous role for sphingolipids in the regulation of NMJ structure.

a-c. Glial expression of lace under the control of the glial driver Repo-Gal4 rescues morphological defects in lace mutant NMJ's including reduced bouton number (b) and increased bouton size (c). ANOVA; $p < .001$ with post hoc Dunnett's comparison to wildtype: *** $p < .001$ and Tukey comparison within groups ### $p < .001$,

References

Aberle H, Haghighi AP, Fetter RD, McCabe BD, Magalhães TR, Goodman CS. 2002. wishful thinking encodes a BMP type II receptor that regulates synaptic growth in Drosophila. Neuron 33:545–558.

Adachi-Yamada T, Gotoh T, Sugimura I, Tateno M, Nishida Y, Onuki T, Date H. 1999. De novo synthesis of sphingolipids is required for cell survival by down-regulating c-Jun N-terminal kinase in Drosophila imaginal discs. Molecular and Cellular Biology 19:7276–7286.

Arima M, Cui D, Kimura T, Sonoda K-H, Ishibashi T, Matsuda S, Ikeda E. 2016. Basigin can be a therapeutic target to restore the retinal vascular barrier function in the mouse model of diabetic retinopathy. Sci Rep 6:38445.

Ashburner M. 1982. The genetics of a small autosomal region of Drosophila melanogaster containing the structural gene for alcohol dehydrogenase. III. Hypomorphic and hypermorphic mutations affecting the expression of hairless. Genetics 101:447–459.

Bejaoui K, Wu C, Scheffler MD, Haan G, Ashby P, Wu L, de Jong P, Brown RH.

2001. SPTLC1 is mutated in hereditary sensory neuropathy, type 1. Nat Genet 27:261–262.

Besse F, Mertel S, Kittel RJ, Wichmann C, Rasse TM, Sigrist SJ, Ephrussi A. 2007. The Ig cell adhesion molecule Basigin controls compartmentalization and vesicle release at Drosophila melanogaster synapses. The Journal of Cell Biology 177:843–855.

Beumer KJ, Rohrbough J, Prokop A, Broadie K. 1999. A role for PS integrins in morphological growth and synaptic function at the postembryonic neuromuscular junction of Drosophila. Development 126:5833–5846.

Brusés JL, Chauvet N, Rutishauser U. 2001. Membrane lipid rafts are necessary for the maintenance of the (alpha)7 nicotinic acetylcholine receptor in somatic spines of ciliary neurons. Journal of Neuroscience 21:504–512.

Chamberlain LH, Burgoyne RD, Gould GW. 2001. SNARE proteins are highly enriched in lipid rafts in PC12 cells: implications for the spatial control of exocytosis. Proc Natl Acad Sci USA 98:5619–5624.

Chan JP, Hu Z, Sieburth D. 2012. Recruitment of sphingosine kinase to presynaptic terminals by a conserved muscarinic signaling pathway promotes neurotransmitter release. Genes Dev 26:1070–1085.

Chan JP, Sieburth D. 2012. Localized sphingolipid signaling at presynaptic terminals is regulated by calcium influx and promotes recruitment of priming factors. Journal of Neuroscience 32:17909–17920.

Ciarlo L, Manganelli V, Garofalo T, Matarrese P, Tinari A, Misasi R, Malorni W, Sorice M. 2010. Association of fission proteins with mitochondrial raft-like domains. Cell Death Differ 17:1047–1058.

Collins CA, Wairkar YP, Johnson SL, DiAntonio A. 2006. Highwire Restrains Synaptic Growth by Attenuating a MAP Kinase Signal. Neuron 51:57–69.

Curtin KD, Meinertzhagen IA, Wyman RJ. 2005. Basigin (EMMPRIN/CD147) interacts with integrin to affect cellular architecture. J Cell Sci 118:2649–2660.

Darios F, Wasser C, Shakirzyanova A, Giniatullin A, Goodman K, Munoz-Bravo JL, Raingo J, Jorgacevski J, Kreft M, Zorec R, Rosa JM, Gandia L, Gutiérrez LM, Binz T, Giniatullin R, Kavalali ET, Davletov B. 2009. Sphingosine facilitates SNARE complex assembly and activates synaptic vesicle exocytosis. Neuron 62:683–694.

Dawkins JL, Hulme DJ, Brahmbhatt SB, Auer-Grumbach M, Nicholson GA. 2001. Mutations in SPTLC1, encoding serine palmitoyltransferase, long chain base subunit-1, cause hereditary sensory neuropathy type I. Nat Genet 27:309–

312.

Deinhardt K, Berninghausen O, Willison HJ, Hopkins CR, Schiavo G. 2006. Tetanus toxin is internalized by a sequential clathrin-dependent mechanism initiated within lipid microdomains and independent of epsin1. The Journal of Cell Biology 174:459–471.

Derry DM, Wolfe LS. 1967. Gangliosides in isolated neurons and glial cells. Science 158:1450–1452.

Dodge FA, Rahamimoff R. 1967. Co-operative action a calcium ions in transmitter release at the neuromuscular junction. J Physiol (Lond) 193:419–432.

Fernandez-Funez P, Casas-Tinto S, Zhang Y, Gómez-Velazquez M, Morales-Garza MA, Cepeda-Nieto AC, Castilla J, Soto C, Rincon-Limas DE. 2009. In vivo generation of neurotoxic prion protein: role for hsp70 in accumulation of misfolded isoforms. PLoS Genet 5:e1000507.

Grass GD, Tolliver LB, Bratoeva M, Toole BP. 2013. CD147, CD44, and the epidermal growth factor receptor (EGFR) signaling pathway cooperate to regulate breast epithelial cell invasiveness. Journal of Biological Chemistry 288:26089–26104.

Grimm MOW, Grimm HS, Pätzold AJ, Zinser EG, Halonen R, Duering M, Tschäpe JA, De Strooper B, Müller U, Shen J, Hartmann T. 2005. Regulation of cholesterol and sphingomyelin metabolism by amyloid-beta and presenilin. Nat Cell Biol 7:1118–1123.

Guan Z, Bykhovskaia M, Jorquera RA, Sutton RB, Akbergenova Y, Littleton JT. 2017. A synaptotagmin suppressor screen indicates SNARE binding controls the timing and Ca(2+) cooperativity of vesicle fusion. Elife 6:2423.

Hering H, Lin C-C, Sheng M. 2003. Lipid rafts in the maintenance of synapses, dendritic spines, and surface AMPA receptor stability. Journal of Neuroscience 23:3262–3271.

Herr DR, Fyrst H, Phan V, Heinecke K, Georges R, Harris GL, Saba JD. 2003. Sply regulation of sphingolipid signaling molecules is essential for Drosophila development. Development 130:2443–2453.

Kacher Y, Futerman AH. 2006. Genetic diseases of sphingolipid metabolism: pathological mechanisms and therapeutic options. FEBS Letters 580:5510–5517.

Koh T-W, Verstreken P, Bellen HJ. 2004. Dap160/intersectin acts as a stabilizing scaffold required for synaptic development and vesicle endocytosis. Neuron 43:193–205.

Krebs S, Medugorac I, Röther S, Strässer K, Förster M. 2007. A missense mutation in the 3-ketodihydrosphingosine reductase FVT1 as candidate causal mutation for bovine spinal muscular atrophy. Proc Natl Acad Sci USA 104:6746–6751.

Lahiri S, Futerman AH. 2007. The metabolism and function of sphingolipids and glycosphingolipids. Cell Mol Life Sci 64:2270–2284.

Lang T, Bruns D, Wenzel D, Riedel D, Holroyd P, Thiele C, Jahn R. 2001. SNAREs are concentrated in cholesterol-dependent clusters that define docking and fusion sites for exocytosis. EMBO J 20:2202–2213.

Lnenicka GA, Keshishian H. 2000. Identified motor terminals in Drosophila larvae show distinct differences in morphology and physiology. J Neurobiol 43:186–197.

Lnenicka GA, Theriault K, Monroe R. 2006. Sexual differentiation of identified motor terminals in Drosophila larvae. J Neurobiol 66:488–498.

Mammucari C, Raffaello A, Vecellio Reane D, Gherardi G, De Mario A, Rizzuto R. 2018. Mitochondrial calcium uptake in organ physiology: from molecular mechanism to animal models. Pflugers Arch. doi: 10.1007/s00424-018-2123-2

Marie B, Sweeney ST, Poskanzer KE, Roos J, Kelly RB, Davis GW. 2004. Dap160/intersectin scaffolds the periactive zone to achieve high-fidelity endocytosis and normal synaptic growth. Neuron 43:207–219.

Marrus SB, Portman SL, Allen MJ, Moffat KG, DiAntonio A. 2004. Differential localization of glutamate receptor subunits at the Drosophila neuromuscular junction. Journal of Neuroscience 24:1406–1415.

Mauch DH, Nägler K, Schumacher S, Göritz C, Müller EC, Otto A, Pfrieger FW. 2001. CNS synaptogenesis promoted by glia-derived cholesterol. Science 294:1354–1357.

McCabe BD, Hom S, Aberle H, Fetter RD, Marqués G, Haerry TE, Wan H, O'Connor MB, Goodman CS, Haghighi AP. 2004. Highwire regulates presynaptic BMP signaling essential for synaptic growth. Neuron 41:891–905.

McLachlan EM, Martin AR. 1981. Non-linear summation of end-plate potentials in the frog and mouse. J Physiol (Lond) 311:307–324.

Milton VJ, Jarrett HE, Gowers K, Chalak S, Briggs L, Robinson IM, Sweeney ST. 2011. Oxidative stress induces overgrowth of the Drosophila neuromuscular junction. Proc Natl Acad Sci USA 108:17521–17526.

Munro S. 2003. Lipid rafts: elusive or illusive? Cell 115:377–388.

Nishiki T, Tokuyama Y, Kamata Y, Nemoto Y, Yoshida A, Sato K, Sekiguchi M, Takahashi M, Kozaki S. 1996. The high-affinity binding of Clostridium botulinum type B neurotoxin to synaptotagmin II associated with gangliosides GT1b/GD1a. FEBS Letters 378:253–257.

Oswald MCW, West RJH, Lloyd-Evans E, Sweeney ST. 2015. Identification of dietary alanine toxicity and trafficking dysfunction in a Drosophila model of hereditary sensory and autonomic neuropathy type 1. Hum Mol Genet 24:6899–6909.

Penno A, Reilly MM, Houlden H, Laurá M, Rentsch K, Niederkofler V, Stoeckli ET, Nicholson G, Eichler F, Brown RH, Eckardstein von A, Hornemann T. 2010. Hereditary sensory neuropathy type 1 is caused by the accumulation of two neurotoxic sphingolipids. Journal of Biological Chemistry 285:11178–11187.

Powers AS, Grizzaffi J, Ribchester R, Lnenicka GA. 2016. Regulation of quantal currents determines synaptic strength at neuromuscular synapses in larval Drosophila. Pflugers Arch 468:2031–2040.

Rawson JM, Lee M, Kennedy EL, Selleck SB. 2003. Drosophila neuromuscular synapse assembly and function require the TGF-β type I receptor saxophone and the transcription factor Mad. J Neurobiol 55:134–150.

Ribchester RR. 2011. Quantal Analysis of Endplate Potentials in Mouse Flexor Digitorum Brevis Muscle. Curr Protoc Mouse Biol 1:429–444.

Roberts M, Willison H, Vincent A, Newsom-Davis J. 1994. Serum factor in Miller-Fisher variant of Guillain-Barré syndrome and neurotransmitter release. Lancet 343:454–455.

Sabourdy F, Astudillo L, Colacios C, Dubot P, Mrad M, Ségui B, Andrieu-Abadie N, Levade T. 2015. Monogenic neurological disorders of sphingolipid metabolism. Biochim Biophys Acta 1851:1040–1051.

Salaün C, Gould GW, Chamberlain LH. 2005. Lipid raft association of SNARE proteins regulates exocytosis in PC12 cells. J Biol Chem 280:19449–19453.

Sasamura T, Matsuno K, Fortini ME. 2013. Disruption of Drosophila melanogaster lipid metabolism genes causes tissue overgrowth associated with altered developmental signaling. PLoS Genet 9:e1003917.

Schmidt N, Kollewe A, Constantin CE, Henrich S, Ritzau-Jost A, Bildl W, Saalbach A, Hallermann S, Kulik A, Fakler B, Shulte U. 2017. Neuroplastin and Basigin are essential auxiliary subunits of plasma membrane Ca^{2+}-ATPases and key regulators of Ca^{2+} clearance. Neuron. 96:827-838

Schuster CM, Davis GW, Fetter RD, Goodman CS. 1996. Genetic dissection of structural and functional components of synaptic plasticity. I. Fasciclin II controls synaptic stabilization and growth. Neuron 17:641–654.

Shen H, Giordano F, Wu Y, Chan J, Zhu C, Milosevic I, Wu X, Yao K, Chen B, Baumgart T, Sieburth D, De Camilli P. 2014. Coupling between endocytosis and sphingosine kinase 1 recruitment. Nat Cell Biol 16:652–662.

Simpson MA, Cross H, Proukakis C, Priestman DA, Neville DCA, Reinkensmeier G, Wang H, Wiznitzer M, Gurtz K, Verganelaki A, Pryde A, Patton MA, Dwek RA, Butters TD, Platt FM, Crosby AH. 2004. Infantile-onset symptomatic epilepsy syndrome caused by a homozygous loss-of-function mutation of GM3 synthase. Nat Genet 36:1225–1229.

Sweeney ST, Davis GW. 2002. Unrestricted Synaptic Growth in spinster—a Late Endosomal Protein Implicated in TGF-β-Mediated Synaptic Growth Regulation. Neuron 36:403–416.

Vital A, Vital C. 2012. Mitochondria and peripheral neuropathies. J Neuropathol Exp Neurol 71:1036–1046.

Wan HI, DiAntonio A, Fetter RD, Bergstrom K, Strauss R, Goodman CS. 2000. Highwire Regulates Synaptic Growth in Drosophila. Neuron 26:313–329.

West RJH, Lu Y, Marie B, Gao F-B, Sweeney ST. 2015. Rab8, POSH, and TAK1 regulate synaptic growth in a Drosophila model of frontotemporal dementia. The Journal of Cell Biology 208:931–947.

Willison HJ, O'Hanlon G, Paterson G, O'Leary CP, Veitch J, Wilson G, Roberts M, Tang T, Vincent A. 1997. Mechanisms of action of anti-GM1 and anti-GQ1b ganglioside antibodies in Guillain-Barré syndrome. J Infect Dis 176 Suppl 2:S144–9.

Zhai L, Chaturvedi D, Cumberledge S. 2004. Drosophila wnt-1 undergoes a hydrophobic modification and is targeted to lipid rafts, a process that requires porcupine. J Biol Chem 279:33220–33227.

Zitman FMP, Todorov B, Furukawa K, Furukawa K, Willison HJ, Plomp JJ. 2010. Total ganglioside ablation at mouse motor nerve terminals alters neurotransmitter release level. Synapse 64:335–338.

Zitman FMP, Todorov B, Jacobs BC, Verschuuren JJ, Furukawa K, Willison HJ, Plomp JJ. 2008. Neuromuscular synaptic function in mice lacking major subsets of gangliosides. Neuroscience 156:885–897.

Zitman FMP, Todorov B, Verschuuren JJ, Jacobs BC, Furukawa K, Furukawa K, Willison HJ, Plomp JJ. 2011. Neuromuscular synaptic transmission in aged ganglioside-deficient mice. Neurobiol Aging 32:157–167.

Zito K, Parnas D, Fetter RD, Isacoff EY, Goodman CS. 1999. Watching a synapse grow: noninvasive confocal imaging of synaptic growth in Drosophila. Neuron 22:719–729.

A

	lace ^{k05305}	*lace* ^{k00706}	*lace* ^{1}	*lace* ^{8}	*lace* ^{2}
lace ^{k05305}	3rd Instar/Pupae	3rd Instar/Pupae	Adult (35%)	Adult (32%)	Adult (33%)
lace ^{k00706}	-	-	Embryo/1st Instar	Adult (29%)	Embryo/1st Instar
lace ^{1}	-	-	-	Adult (32%)	Embryo/1st Instar
lace ^{8}	-	-	-	-	Embryo/1st Instar
lace ^{2}	-	-	-	-	-

B

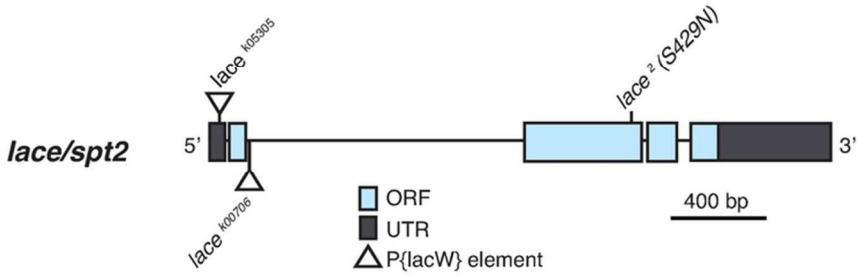

Figure 1. lace is Essential for Survival in Drosophila

73x54mm (300 x 300 DPI)

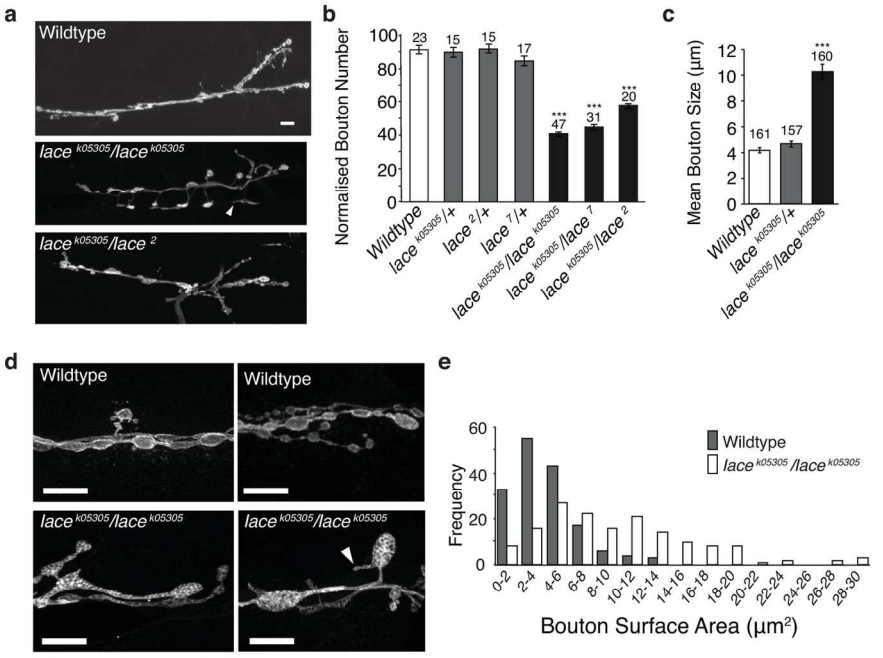

Figure 2. Loss of Sphingolipid Synthesis Leads to Enlarged Bouton Structure at the NMJ

143x114mm (300 x 300 DPI)

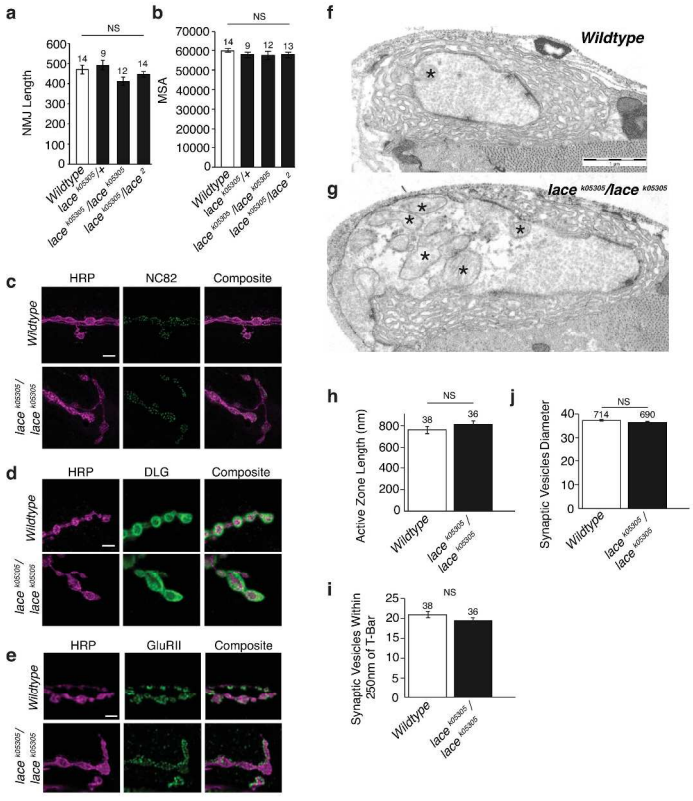

Figure 3. Synaptic Components Appear Unchanged in lace Mutants

302x418mm (300 x 300 DPI)

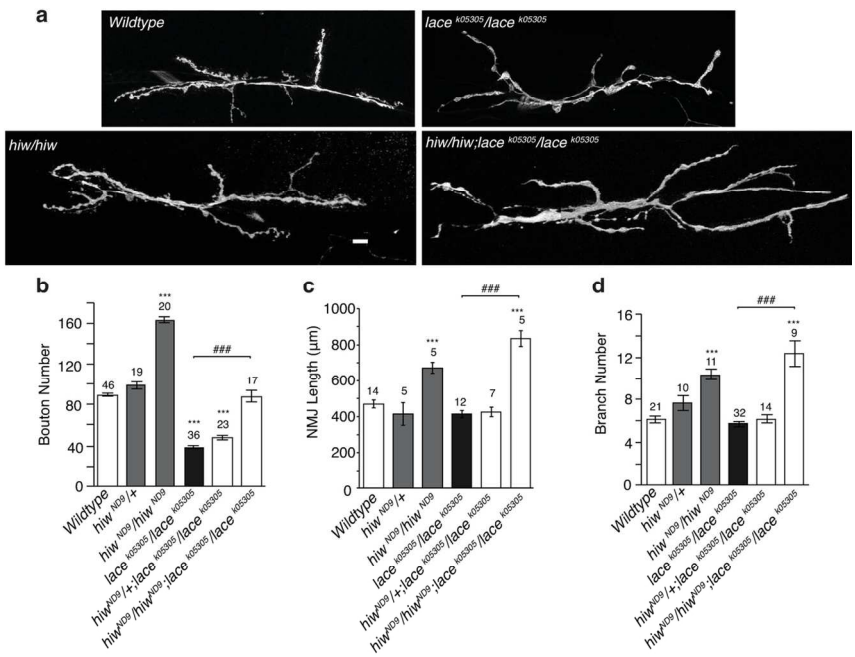

Figure 4. lace Mutants Are Capable of Further Synaptic Growth.

127x83mm (300 x 300 DPI)

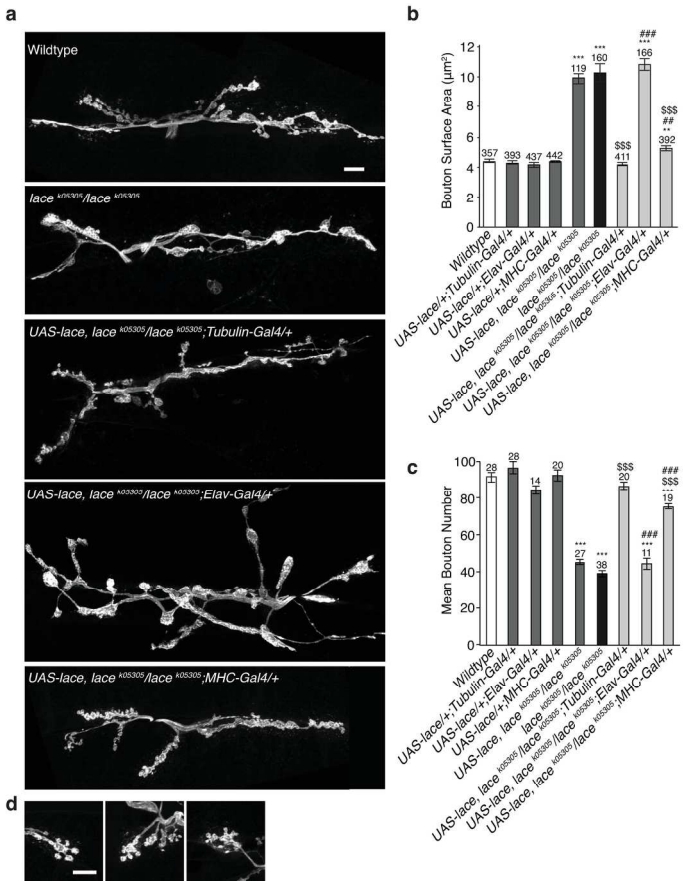

Figure 5. Aberrant Synaptic Architecture Can be partially Alleviated by Post- Expression of lace

187x164mm (300 x 300 DPI)

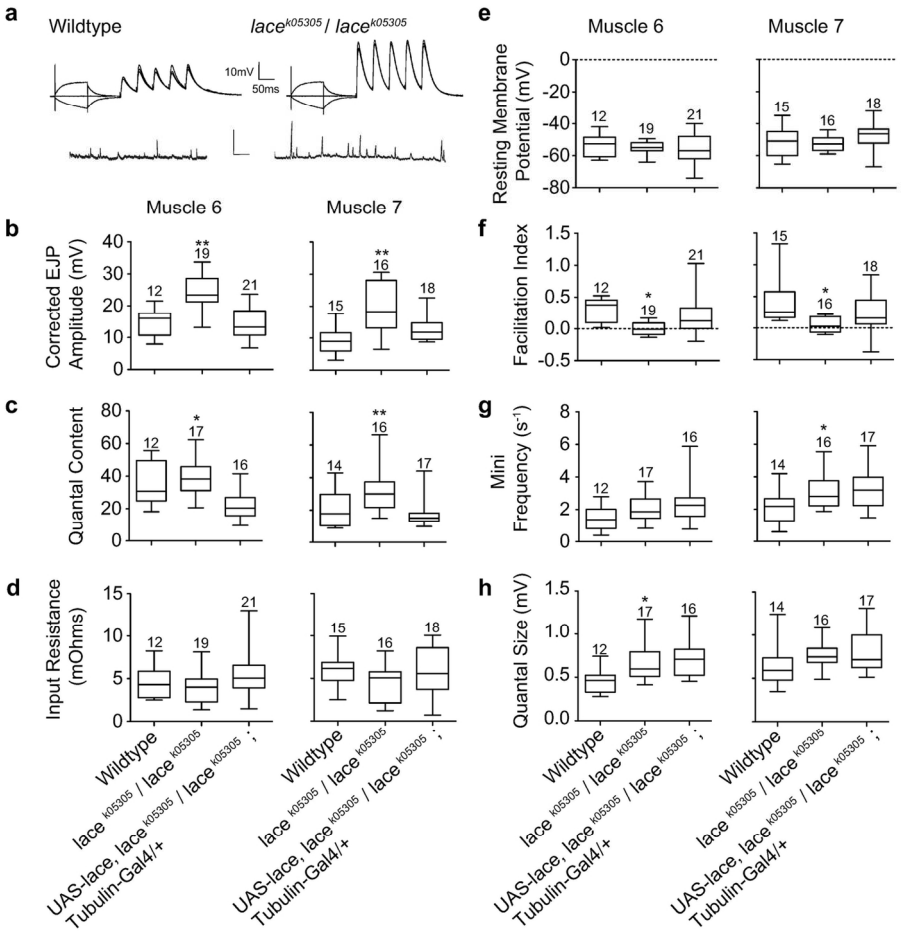

Figure 6. lace mutants display increased synaptic strength

139x130mm (300 x 300 DPI)

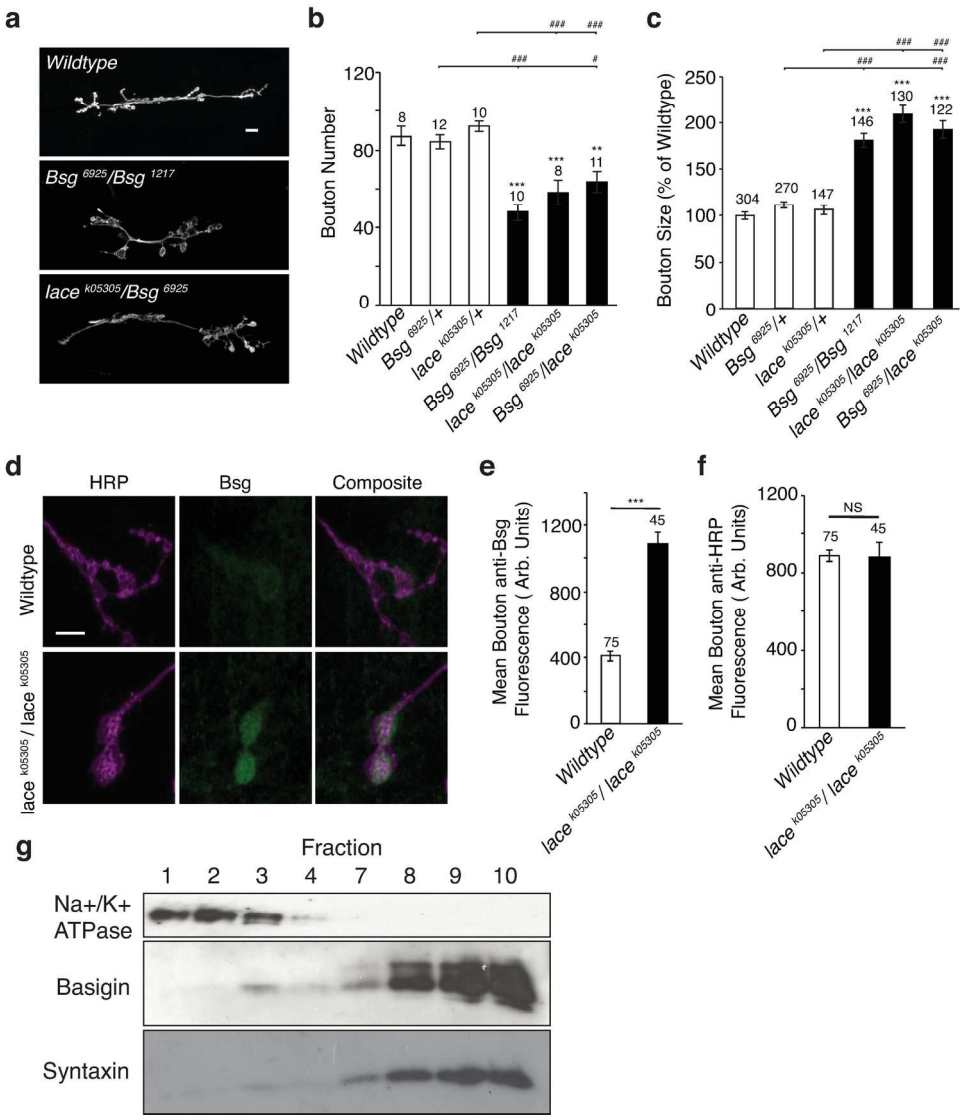

Figure 7. lace Mutants Reveal a Functional Interaction Between Between lace and Basigin

166x185mm (300 x 300 DPI)

Supplementary

Supplementary Table 1. Antibodies

Antibody	Immunogen	Manufacturer, Catalogue number, Species, RIDD	Concentration
Anti-HRP (Cy3 Conjugated)	Horseradish Peroxidase	Jackson ImmunoResearch Labs Cat# 123-165-021 RRID:AB_2338959, Goat, Polyclonal	1:200
Anti-Synaptotagmin	*Drosophila* Recombinant GST-dSyt1	Sweeney Lab, (West et al., 2015), Rabbit, Polyclonal, RRID:AB_2713991	1:2000
Anti-NC82/Bruchpilot	*Drosophila* C-terminal aa 1227-1740	DSHB Cat# nc82 RRID:AB_2314867 Mouse, Monoclonal	1:50
Anti-DLG	*Drosophila* aa 439-756	DSHB Cat# 4F3 anti-discs large RRID:AB_528203, Mouse, Monoclonal	1:50
Anti-GluRIIB	15 C-terminal residues (-ASSAKKKKTRRIEK) of predicted dGluRIIB	Marrus et al., (2004), Rabbit, Polyclonal	1:2500
Anti-Basigin	N-terminal synthetic peptide (QSLDKLVPNYD)	Besse et al., (2007), Rat, Polyclonal	1:200
Anti-Syntaxin	*Drosophila* Syntaxin	DSHB Cat# 8c3 RRID:AB_528484, Mouse, Monoclonal	1:50
Anti-Na+/K+ ATPase	Chicken ATPase, (Na(+) K(+) alpha subunit	DSHB Cat# a5 RRID:AB_2166869, Mouse, Monoclonal	1:100,000
HRP Conjugated anti-Mouse		Cell Signaling Technology Cat# 7076 RRID:AB_330924, horse, polyclonal	1:1000
HRP Conjugated anti-Rat		Cell Signaling Technology Cat# 7077 RRID:AB_10694715, goat, polyclonal	1:1000

Supplementary Table 2.

Muscle 6	EM (mV)	Rin (MΩ)	mEJP (mV)	mEJP f (s^{-1})	Corrected EJP (mV)	M1 (quanta)	Facilitation Index (m5/m-1)
Wildtype	-53.4	4.56	0.46	1.45	14.8	34.6	0.31
N=8 larvae n=12 muscles	(-57.6, -49.2)	(3.42, 5.70)	(0.37, 0.55)	(0.96, 1.95)	(12.2, 17.5)	(26.0, 43.2)	(0.19, 0.43)
$lace^5$/ $lace^5$	-55.4	4.06	0.65*	2.05	24.5**	39.3*	0.00*
N=8 larvae n=19 muscles	(-57.4, -53.4)	(3.15, 4.98)	(0.55, 0.76)	(1.62, 2.47)	(21.7, 27.2)	(33.7, 44.9)	(-0.04, 0.05)
$lace^5$/ $lace^5$,UAS-lace;Tubulin-Gal4	-53.3	5.27	0.7	2.4	14.2	21.3	0.19
N=8 larvae n= 21 muscles	(-58.4, -48.2)	(4.12, 6.42)	(0.59, 0.80)	(1.71, 3.08)	(12.0, 16.3)	(17.1, 25.6)	(0.03, 0.35)

ANOVA with post-hoc Tukey comparison between groups

* P<0.05 compared with either Wildtype or Rescue

** P<0.05 compared with both Wildtype and Rescue

Supplementary Table 3.

Muscle 7	EM (mV)	Rin (MΩ)	mEJP (mV)	mEJP f (s^{-1})	Corrected EJP (mV)	M1 (quanta)	Facilitation Index (m5/m-1)
Wildtype	-51.8	5.983	0.62	1.06	14.8	20.9	0.43
N=8 larvae n=15 muscles	(-56.7, -46.9)	(4.90, 7.07)	(0.49, 0.74)	(0.79, 1.33)	(12.2, 17.5)	(14.6, 27.2)	(0.23, 0.64)
$lace^5$/ $lace^5$	-52.8	4.38	0.75	1.54*	23.8**	32.9**	0.04*
N=8 larvae n=16 muscles	(-55.3, -50.4)	(3.26, 5.51)	(0.67, 0.84)	(1.26, 1.83)	(19.1, 28.6)	(24.7, 41.0)	(-0.02, 0.11)
$lace^5$/ $lace^5$,UAS-lace;Tubulin-Gal4	-48.3	5.94	0.81	1.63	12.6	17.1	0.22
N= 8 larvae n=20 muscles	(-53.2, -43.4)	(4.62, 7.25)	(0.68, 0.93)	(1.33, 1.94)	(11.0, 14.7)	(13.2, 21.0)	(0.05, 0.38)

ANOVA with post-hoc Tukey comparison between groups

* P<0.05 compared with either Wildtype or Rescue

** P<0.05 compared with both Wildtype and Rescue

a

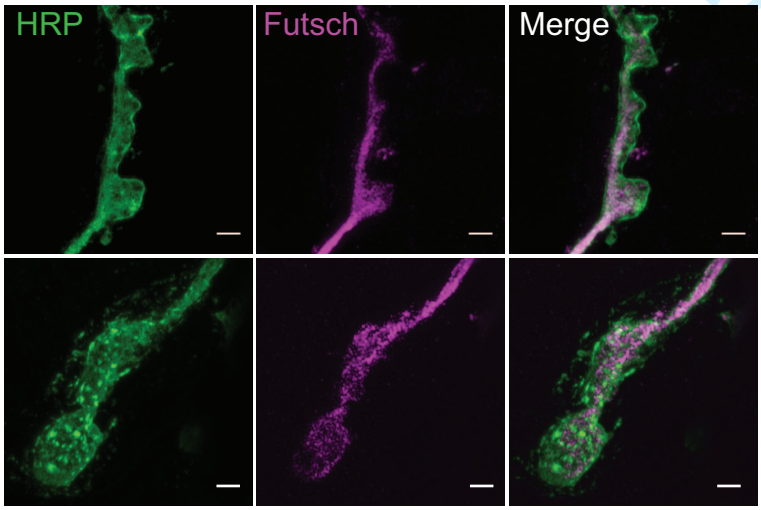

b